Semiclassical spectrum of integrable systems in a magnetic field

D Spehner†, R Narevich and E Akkermans

Department of Physics, Technion, 32000 Haifa, Israel

Abstract. The quantum dynamics of an electron in a uniform magnetic field is studied for two-dimensional geometries corresponding to integrable cases. The WKB approximations of the energies and the eigenfunctions of the semi-infinite plane and the disk are obtained. These analytical solutions are shown to be in excellent agreement with the numerical results obtained from the Schrödinger equations even for the lowest levels. It is shown for strong fields that the coalescence of the caustics with the boundary has to be taken into account in order to describe the gradual transition in the spectrum from Landau-like levels into edge levels.

1. Introduction

The aim of this work is to present some analytical methods to obtain the energy spectrum and eigenfunctions of non-interacting electrons constrained to a two-dimensional domain with boundaries and submitted to a uniform perpendicular magnetic field.

This problem is relevant to various situations in condensed matter physics. In the low magnetic field regime, defined by the condition $\Phi \ll \Phi_0$, where Φ is the magnetic flux through the system and $\Phi_0 = hc/e$ is the quantum flux, recent experiments [1] performed on small metallic systems showed the importance of the effect of the boundaries. It actually determines the nature of the zero-field classical motion being either integrable or chaotic. The magnetic susceptibility has been shown using numerical and semiclassical methods to present large fluctuations and to be reduced with respect to the Landau value in the chaotic case, whereas it is enhanced in the integrable case [2, 3]. In the opposite limit $\Phi \gg \Phi_0$ of high fields, we are in the so-called integer quantum Hall effect (IQHE) regime, where the edge states associated with the boundary play a prominent role [4]. In this work, we shall concentrate on the problem of non-interacting electrons constrained by hard walls to move on the semi-infinite plane or on a disk.

The classical dynamics allows for a natural distinction between bulk and edge states. A first semiclassical method is based on the Einstein–Brillouin–Keller (EBK) quantization rules [5] and preserves this bulk and edge states splitting, by giving different quantization rules for each of them. This approximation is further improved for the semi-infinite plane by constructing the asymptotically matched WKB wavefunction and then finding its zeros corresponding to the energy levels. The calculation is not new [6], however we present it in detail, as it serves as a starting point for the WKB approximation for the disk. The spectrum and eigenfunctions of the disk are found using the comparison equation method

---

† Present address: Institut de Recherche sur les Systèmes Atomiques et Moléculaires Complexes (IRSAMC), Université Paul Sabatier, 118 route de Narbonne, Toulouse Cedex 04, France.
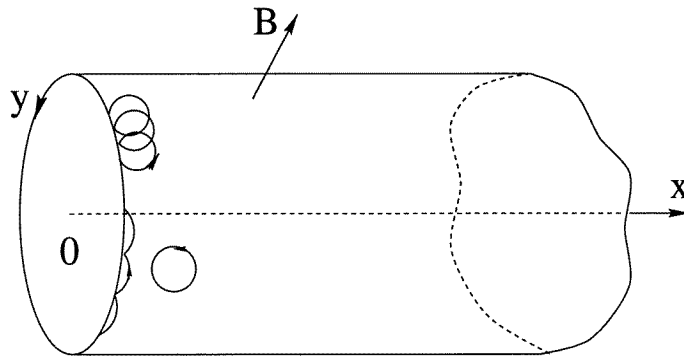
Figure 1. Semi-infinite cylinder in the magnetic field B.

(for general references, see [7, 8]), also called the Miller–Good method [9], which is used to map the problem onto the semi-infinite plane's one. The semiclassical results obtained are found by comparison with numerical calculations to give surprisingly good approximations of the lowest levels. They are valid for any strength of the magnetic field, thus providing us with a way to study more particularly both the IQHE and the low-field regimes.

2. The semi-infinite plane in the magnetic field

In this section the spectrum of an electron in the semi-infinite plane in a magnetic field is approximated, first by using the EBK quantization rules and then by building the matched WKB wavefunction. To introduce the semiclassical language, we begin by considering the classical dynamics.

2.1. The classical dynamics

We consider a spinless particle of charge $-e$ ($e > 0$) and mass m constrained by a hard wall to move in the semi-infinite plane. A uniform magnetic field B is applied perpendicular to the plane. Cartesian coordinates are defined such that the x-axis is perpendicular to the boundary and the motion is confined to positive values of x. It will be convenient to consider the boundary having a finite length L and therefore we impose periodic boundary conditions in the y-direction. The particle can then be regarded as if it moves on the semi-infinite cylinder represented in figure 1.

In the Landau gauge $\boldsymbol{A} = (0, Bx)$, the Hamiltonian of the particle is:

$$H = \frac{1}{2m}\left(p_x{}^2 + \left(p_y + \frac{e}{c}Bx\right)^2\right). \tag{1}$$

The momentum is $\boldsymbol{p} = (m\dot{x}, m\dot{y} - eBx/c)$. The total energy E and the y-component p_y of the momentum are constants of motion, therefore the problem is integrable. In the four-dimensional phase space of the Cartesian coordinates and the corresponding momenta, each family of classical trajectories are winding on an invariant torus defined by the two constants of motion. The ensemble of trajectories splits naturally into two families: those that do not touch the boundary (bulk trajectories), and others (edge trajectories). Bulk trajectories of energy E go anticlockwise in circles of radius $r_c = \sqrt{2E/m\omega^2}$ (where $\omega = eB/mc$ is the cyclotron frequency) with their centre farther than r_c from the edge. They have momenta $p_y < -\sqrt{2mE}$. Edge trajectories have momenta $-\sqrt{2mE} < p_y < \sqrt{2mE}$ and undergo

specular reflections on the boundary before closing a circle so that the cyclotron orbit centre begins drifting along the edge (see figure 1). Increasing p_y at fixed energy, the bulk tori in phase space are transformed at $p_y = -\sqrt{2mE}$ in a discontinuous way into edge tori.

2.2. The EBK quantization

We now consider the quantum-mechanical version of the same problem. Dirichlet boundary conditions are imposed on the wavefunction $\Psi(x, y)$:

$$\Psi(0, y) = 0. \tag{2}$$

The application of the EBK quantization rules for integrable systems leads to the quantization of the two action variables I_y and I_x. The action I_y corresponding to the motion along the y-axis (parallel to the boundary) is quantized by:

$$I_y = \frac{1}{2\pi} \oint p_y \, \mathrm{d}y = \frac{p_y L}{2\pi} = n_y \hbar \tag{3}$$

with $n_y \in \mathbb{Z}$. The motion along the x-axis (perpendicular to the boundary) is different for the bulk and edge states, therefore their quantization also differs. The energies of the bulk states are found from

$$I_x = \frac{1}{2\pi} \oint p_x \, \mathrm{d}x = \frac{1}{\pi} \int_0^{2r_c} \mathrm{d}x \sqrt{2mE - \left(p_y + \frac{e}{c}Bx\right)^2} = \frac{E}{\omega} = \hbar \left(n_x + \frac{1}{2}\right) \tag{4}$$

where $n_x \in \mathbb{N}$. For the edge states the EBK quantization gives

$$I_x = I_x(\xi_0) = \frac{1}{\pi} \int_0^{r_c - \frac{p_y}{m\omega}} \mathrm{d}x \sqrt{2mE - \left(p_y + \frac{e}{c}Bx\right)^2}$$

$$= \frac{2E}{\pi\omega} \int_{\xi_0 - 1}^0 \mathrm{d}\xi \sqrt{-\xi(\xi + 2)} = \hbar(n_x + \tfrac{3}{4}) \tag{5}$$

where

$$\xi_0 = \frac{p_y}{m\omega r_c} = \frac{2\pi n_y \hbar}{L\sqrt{2mE}}. \tag{6}$$

For the bulk trajectories ($\xi_0 < -1$), the Maslov index is $\frac{1}{2}$; we obtain degenerate Landau levels $E = \hbar\omega(n_x + \frac{1}{2})$ which correspond to states that are completely insensitive to the presence of the boundary. For the edge trajectories ($|\xi_0| < 1$), the integration range is restricted because of the reflection from the boundary, and the Maslov index is $\frac{3}{4}$ since there is one turning point (Maslov index $\frac{1}{4}$) and one reflection (Maslov index $\frac{1}{2}$ associated to a change of sign of the wavefunction). The energies are solutions of (5) and (6). They are non-degenerate and bounded below by $\hbar\omega(n_x + \frac{3}{4})$ for each n_x. Note that $E \to \infty$ when $\xi_0 \to 1$. There is a singularity in the EBK spectrum, separating bulk and edge energies. This result is clearly incorrect: as noted in [4], the energy levels should rise steadily from values close to the Landau levels up to infinity.

2.3. Matching the WKB wavefunctions

Once the motion in the y-direction is integrated, the Schrödinger equation together with the boundary condition (2) reduces to a one-dimensional Sturm–Liouville problem. A systematic WKB analysis is well developed for those kinds of problems and improves the preceding EBK approach.

We introduce the dimensionless variables $\tilde{x} = \sqrt{2}x/l_B$ and $\tilde{x}_0 = \sqrt{2}p_y/m\omega l_B$, where $l_B = \sqrt{\hbar c/eB}$ is the magnetic length. Using (1), the Schrödinger equation for the one-dimensional wavefunction $\varphi(\tilde{x}) = e^{-ip_y y/\hbar}\Psi(x, y)$ reads:

$$\left(\frac{d^2}{d\tilde{x}^2} + \frac{E}{\hbar\omega} - \frac{1}{4}(\tilde{x} + \tilde{x}_0)^2\right)\varphi(\tilde{x}) = 0. \tag{7}$$

Let us set $\epsilon = \hbar\omega/2E$. A subsequent change of variable $\xi = \sqrt{\epsilon/2}(\tilde{x}+\tilde{x}_0)-1 = x/r_c+\xi_0-1$ gives:

$$\epsilon^2 f''(\xi) - (\xi^2 + 2\xi)f(\xi) = 0 \tag{8}$$

where $f(\xi) = \varphi(\tilde{x})$. Equation (7) is a Weber equation, and its solution which vanishes at infinity is given (up to an arbitrary constant) by:

$$\varphi(\tilde{x}) = D_{\frac{E}{\hbar\omega}-\frac{1}{2}}(\tilde{x} + \tilde{x}_0) \tag{9}$$

where $D_\nu(u)$ is the parabolic cylinder function [10, 11]. Using (9) and condition (2) one can obtain the spectrum numerically. The Dirichlet boundary condition (2) is

$$\varphi(0) = f(\xi_0 - 1) = 0 \tag{10}$$

in the new variables. Since the solutions f of equation (8) depend only on ϵ, without this condition the energies would be proportional to $\hbar\omega$ (Landau levels). However, this condition makes the rescaled energies $E/\hbar\omega$ depend on the (energy-dependent) parameter ξ_0. They are given by an implicit equation of the form:

$$\frac{E}{\hbar\omega} = \frac{1}{2\epsilon} = h_{n_x}(\xi_0) \tag{11}$$

where ξ_0 is given by (6), and the label n_x refers to different 'energy bands'. In the infinite L limit, $h_{n_x}(\xi_0)$ gives the appropriate energy bands (in this limit ξ_0 varies continuously).

Our purpose in this section is to use a semiclassical approximation in order to find explicit analytical expressions for the energies. As noted by Isihara and Ebina [6], for small ϵ (i.e. large energies), (8) is a standard example of equation where the WKB method is applicable. It has two turning points at $\xi_1 = 0$ and $\xi_2 = -2$. Sufficiently far from them, the WKB function is given by the following asymptotic expression [10]:

$$f_{\text{WKB}}(\xi) = (\xi^2 + 2\xi)^{-1/4}\left(C_+ \exp\left(\frac{1}{\epsilon}\int^\xi d\xi' \sqrt{\xi'(\xi' + 2)}\right)\right.$$
$$\left. + C_- \exp\left(-\frac{1}{\epsilon}\int^\xi d\xi' \sqrt{\xi'(\xi' + 2)}\right)\right) \tag{12}$$

where C_+ and C_- are arbitrary constants. In the vicinity of the turning points this approximation breaks down. The potential $(\xi^2 + 2\xi)$ is then linearized in equation (8) and the resulting Airy equation can be solved exactly. One obtains the approximate solution $f_{\text{WKB}}(\xi)$ by matching the corresponding Airy solutions for each turning point with the WKB solutions (12) valid to the right, between, and to the left of them. This matching procedure has to be accomplished from the right to the left [10].

The function $f_{\text{WKB}}(\xi)$ consists of five branches, related to the five overlapping intervals in which the WKB and Airy approximations are valid.

(i) The first branch has a domain defined by $\xi \gg \epsilon^{2/3}$, where expression (12) holds [10]. The vanishing of the wavefunction at infinity fixes $C_+ = 0$, and we can set arbitrarily $C_- = 1$. Thus, the first branch of the WKB function is:

$$f_{\text{WKB}}^{(1)}(\xi) = (\xi^2 + 2\xi)^{-1/4} \exp\left(-\frac{1}{\epsilon}\int_0^\xi d\xi' \sqrt{\xi'(\xi' + 2)}\right). \tag{13}$$

It is always non-zero, so there are no solutions of (8) and (10) for $\xi_0 - 1 \gg \epsilon^{2/3}$.

(ii) The second branch approximates the exact solution near the first turning point, i.e. for $|\xi| \ll 1$, where $\xi^2 + 2\xi$ can be linearized and replaced by 2ξ in equation (8). It consists therefore of a linear combination of two independent Airy functions $\mathrm{Ai}(t)$ and $\mathrm{Bi}(t)$ with $t = 2^{1/3}\xi/\epsilon^{2/3}$. When ξ is such that $\epsilon^{2/3} \ll \xi \ll \epsilon^{2/5}$, t is large so the asymptotic approximations of Airy functions can be used, and we can approximate the exponential in (13) by $\exp(-2\sqrt{2}\xi^{3/2}/3\epsilon)$. We match for such ξ's the solution of the linearized equation with $f_{\mathrm{WKB}}^{(1)}(\xi)$ and determine the unknown constants of the linear combination. This gives:

$$f_{\mathrm{WKB}}^{(2)}(\xi) = \frac{2\sqrt{\pi}}{(2\epsilon)^{1/6}}\,\mathrm{Ai}\left(\frac{2^{1/3}}{\epsilon^{2/3}}\xi\right). \tag{14}$$

The energies are found by imposing the Dirichlet condition (10) on this solution:

$$\frac{E}{\hbar\omega} = h_{n_x}(\xi_0) = \left(\frac{a_{n_x}}{2\xi_0 - 2}\right)^{3/2} \qquad 0 < 1 - \xi_0 \ll 1 \tag{15}$$

where the a_{n_x} are the $(n_x + 1)$th zeros of the Airy function $\mathrm{Ai}(t)$. These energies are associated with the 'whispering gallery' orbits (see figure 1) which are concentrated in a very narrow region near the boundary. We note that they can be obtained from a 'generalized EBK rule' by letting n_x be such that $n_x + \frac{3}{4} = 2(-a_{n_x})^{3/2}/3\pi$ in (5), instead of an integer. There are no energies for $\xi_0 > 1$, since the real zeros of $\mathrm{Ai}(t)$ are negative.

(iii) Between the two turning points ξ_1 and ξ_2, expression (12) holds again and to determine the constants C_+ and C_- we do the matching with $f_{\mathrm{WKB}}^{(2)}(\xi)$ in the interval $-\epsilon^{2/5} \ll \xi \ll -\epsilon^{2/3}$. This gives for $\xi \ll -\epsilon^{2/3}$ and $\xi + 2 \gg \epsilon^{2/3}$:

$$f_{\mathrm{WKB}}^{(3)}(\xi) = 2(-\xi^2 - 2\xi)^{-1/4}\sin\left(\frac{1}{\epsilon}\int_\xi^0 \mathrm{d}\xi'\,\sqrt{-\xi'(\xi' + 2)} + \frac{\pi}{4}\right). \tag{16}$$

The argument of the sine is $\pi I_x(\xi + 1)/\hbar + \pi/4$, where $I_x(\xi + 1)$ is the classical action (5) for the edge motion, and is also given by the following formula:

$$I_x(\xi + 1) = \frac{\hbar}{2\pi\epsilon}\left(\arccos\xi - \xi\sqrt{1 - \xi^2}\right). \tag{17}$$

Thus, as expected we obtain the EBK quantization (5) for ξ_0 between but not too close to 1 and -1. The comparison of the energies derived within the WKB approximation with the exact ones found numerically is shown in figure 2(a) for the second and third branches.

(iv) This branch represents the function in the vicinity of the second turning point $\xi_2 = -2$. Repeating the scheme of matching with the previous third branch, we obtain for $|\xi + 2| \ll 1$:

$$f_{\mathrm{WKB}}^{(4)}(\xi) = \frac{2\sqrt{\pi}}{(2\epsilon)^{1/6}}\left(\sin\left(\frac{\pi}{2\epsilon}\right)\mathrm{Ai}\left(-\frac{2^{1/3}}{\epsilon^{2/3}}(\xi + 2)\right) + \cos\left(\frac{\pi}{2\epsilon}\right)\mathrm{Bi}\left(-\frac{2^{1/3}}{\epsilon^{2/3}}(\xi + 2)\right)\right). \tag{18}$$

Thus the energies $E/\hbar\omega = 1/2\epsilon$ for $|\xi_0 + 1| \ll \epsilon^{2/3}$ are given by:

$$\tan\frac{\pi}{2\epsilon} = -\frac{\mathrm{Bi}\left(-\frac{2^{1/3}}{\epsilon^{2/3}}(\xi_0 + 1)\right)}{\mathrm{Ai}\left(-\frac{2^{1/3}}{\epsilon^{2/3}}(\xi_0 + 1)\right)}. \tag{19}$$

These energies correspond either to edge trajectories which nearly complete full circles before being reflected or to bulk trajectories nearly touching the boundary (see figure 1). In figure 2(b) we see that, for the lowest band $n_x = 0$, the energies of the fourth branch become closer below $\xi_0 \simeq -0.5$ to the exact energies than those of the third branch.
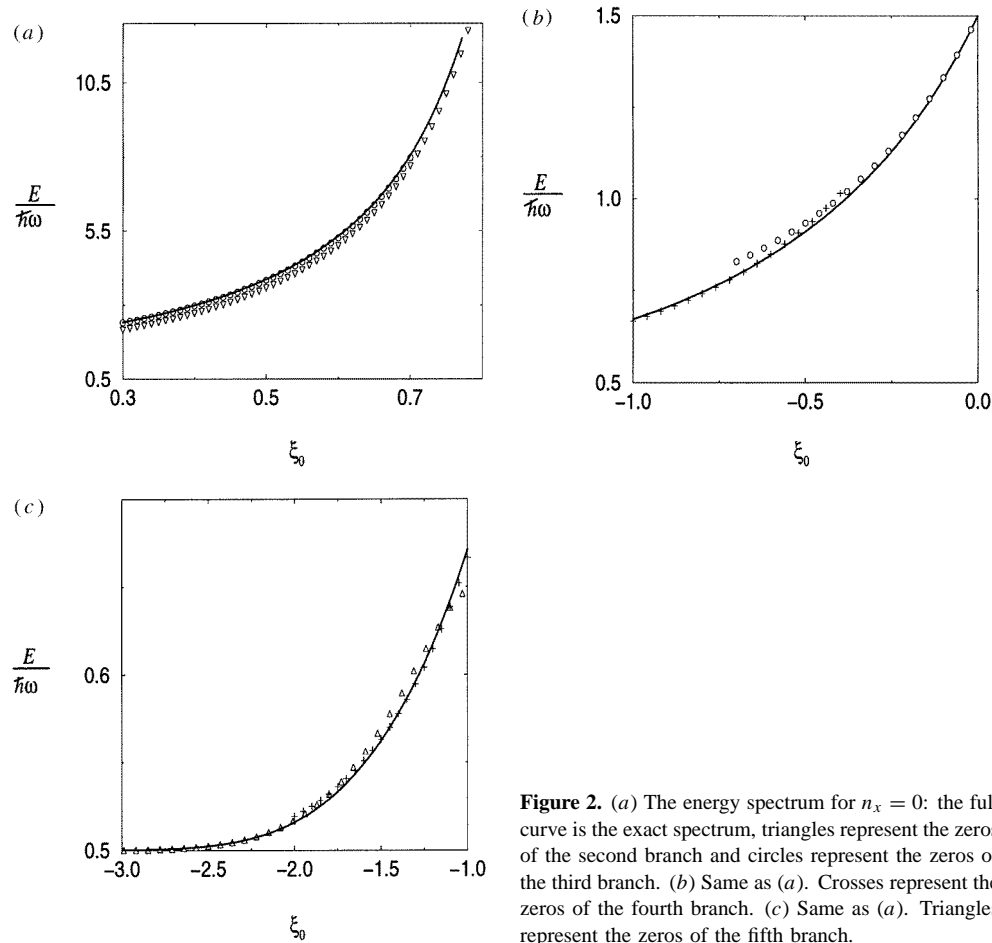
Figure 2. (a) The energy spectrum for $n_x = 0$: the full curve is the exact spectrum, triangles represent the zeros of the second branch and circles represent the zeros of the third branch. (b) Same as (a). Crosses represent the zeros of the fourth branch. (c) Same as (a). Triangles represent the zeros of the fifth branch.

(v) The fifth branch $f_{\text{WKB}}^{(5)}(\xi)$ is derived in a similar way. For $-\xi - 2 \gg \epsilon^{2/3}$:

$$f_{\text{WKB}}^{(5)}(\xi) = (\xi^2 + 2\xi)^{-1/4} \left(\sin\left(\frac{\pi}{2\epsilon}\right) e^{-1/\epsilon \int_\xi^{-2} d\xi' \sqrt{\xi'(\xi'+2)}} + 2\cos\left(\frac{\pi}{2\epsilon}\right) e^{1/\epsilon \int_\xi^{-2} d\xi' \sqrt{\xi'(\xi'+2)}} \right).$$

(20)

The equation to be solved for the energies is:

$$\frac{1}{2} \tan\frac{\pi}{2\epsilon} = -\exp\left(\frac{1}{\epsilon}\left(-\text{arccosh}(-\xi_0) - \xi_0\sqrt{\xi_0^2 - 1} \right) \right) \qquad -\xi_0 - 1 \gg \epsilon^{2/3}.$$

(21)

When $|\xi_0|$ is large, the r.h.s. of this equation is a large number so that the argument of the tangent on the l.h.s. is to a good approximation π time a half-integer. Thus for $|\xi_0|$ sufficiently large, the energies are very close to the Landau levels given by (4), i.e. $1/2\epsilon \simeq n_x + \frac{1}{2}$. The solutions of the energy equations for the fourth and fifth branches and the exact energies are shown in figure 2(c).

The graphs in figures 2(a)–(c) show a very good agreement between the exact calculation and the matched WKB approximation even for the lowest energies. The distinction between the bulk and edge states disappears and the spectrum rises gradually from $\hbar\omega/2$ to infinitely large edge energies.

3. The disk in magnetic field

In this section we study a similar problem to that of the previous section but for a geometry of a disk with centre O and radius R. The magnetic field B is applied in the z-direction perpendicular to the disk. We first discuss the classical dynamics of this system and then compute the semiclassical eigenfunctions and spectrum. Finally, we briefly discuss the charge transport by introducing an Aharonov–Bohm flux line at the origin O.

3.1. Classical dynamics

For the disk geometry, a convenient choice for $\boldsymbol{A}$ is given by the symmetric gauge $\boldsymbol{A} = \frac{1}{2}Br\boldsymbol{e}_\theta$, where (r, θ) are polar coordinates and $\boldsymbol{e}_r$, $\boldsymbol{e}_\theta$ the corresponding unit vectors. The two momenta canonically conjugated to r and θ are $p_r = m\dot{r}$ and $p_\theta = mr^2(\dot{\theta} - \frac{\omega}{2})$, the z-component of the angular momentum. In the symmetric gauge the Hamiltonian of the particle reads:

$$H = \frac{1}{2m}\left(p_r{}^2 + \frac{1}{r^2}\left(p_\theta + \frac{m\omega}{2}r^2\right)^2\right). \tag{22}$$

Since p_θ and the energy E are conserved by reflection on the boundary, we again deal with an integrable system.

Let us introduce the dimensionless radius $\rho_0 = R/r_c$ and momentum $l_z = p_\theta/m\omega r_c^2$, where $r_c = \sqrt{2E/m\omega^2}$ is the cyclotron radius. Setting $H = m\omega^2 r_c^2/2$ in (22) and using the fact that $p_r^2 \geqslant 0$, one can show that l_z has to be smaller than $\frac{1}{2}$, and that trajectories of energy E and angular momentum l_z are inside the annulus $r_{\min} \leqslant r \leqslant r_{\max}$, with $r_{\min} = r_c| - 1 + \sqrt{1 - 2l_z}|$ and $r_{\max} = r_c(1 + \sqrt{1 - 2l_z})$. One must have $r_{\min} \leqslant R$. This implies $-\rho_0^2/2 - \rho_0 \leqslant l_z$. If $\rho_0 \leqslant 1$, the condition $l_z \leqslant -\rho_0^2/2 + \rho_0$ also has to be fulfilled. In the opposite case $\rho_0 > 1$, the trajectories of energy E split into two families: for angular momenta $-\rho_0^2/2 - \rho_0 \leqslant l_z \leqslant -\rho_0^2/2 + \rho_0$, $r_{\max} \geqslant R$ and the particle bounces off the boundary (edge trajectories); for momenta $-\rho_0^2/2 + \rho_0 \leqslant l_z \leqslant \frac{1}{2}$, $r_{\max} \leqslant R$ and the particle follows a circle of radius r_c without touching the boundary (bulk trajectories) (see figure 3). If $\rho_0 \leqslant 1$, all trajectories of energy E are of the edge type. Since in quantum mechanics $\hbar\omega/2$ is a lower bound for the energy of our system, this situation is relevant in particular for disks of radii R smaller than the magnetic length $l_B = \sqrt{\hbar/m\omega}$. This weak field or small system limit has been extensively studied before (see for exampe [3] and references therein).

Trajectories with positive values of angular momenta enclose (and turn around) the origin O (see figure 3). In fact, for such values of l_z, $r_{\max} \leqslant 2r_c$. The value $l_z = 0$ is associated with trajectories having a turning point $r_{\min}$ in the radial direction equal to zero. For $\rho_0 > 1$, the upper value $l_z = \frac{1}{2}$ is associated with bulk trajectories centred on O. Note that the two turning points in the radial direction, $r_{\min}$ and $r_{\max}$, coalesce when $l_z \to \frac{1}{2}-$. In virtue of these classical considerations, one can expect the semiclassical spectrum to differ noticeably for positive and negative values of the angular momentum.

3.2. Semiclassical wavefunction

Let us now formulate the quantum-mechanical problem. Since the system is invariant by rotation along (Oz), we choose wavefunctions $\Psi(r, \theta) = \varphi(r)\mathrm{e}^{\mathrm{i}l\theta}$ having well-defined values $l\hbar$ of the angular momentum along (Oz). $\varphi(r)$ satisfies the radial Schrödinger equation:

$$\left\{-\frac{\hbar^2}{2m}\left(\frac{\mathrm{d}^2}{\mathrm{d}r^2} + \frac{1}{r}\frac{\mathrm{d}}{\mathrm{d}r}\right) + \frac{1}{2mr^2}\left(l\hbar + \frac{m\omega r^2}{2}\right)^2 - E\right\}\varphi(r) = 0. \tag{23}$$
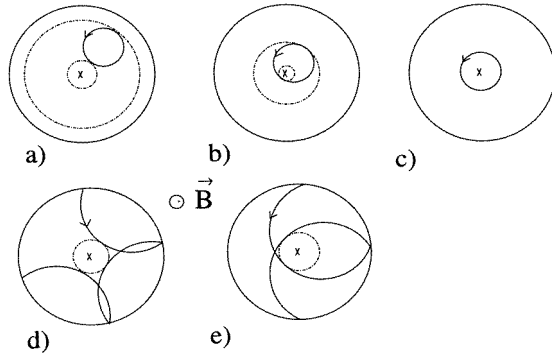
Figure 3. The classical motion for the disk in magnetic field: bulk trajectories are shown in (a)–(c) and edge trajectories in (d),(e). The circles $r = r_{\min}$ and $r = r_{\max}$ are represented with shaded lines. The angular momentum l_z is negative in (a),(d), it is positive in (b),(c),(e) and equal to $\frac{1}{2}$ in (e).

The Dirichlet boundary condition $\varphi(R) = 0$ is imposed on this wavefunction. Equation (23) has an exact solution remaining finite at the origin, given (up to an arbitrary multiplicative constant) by:

$$\varphi(r) = \left(\frac{r}{\lambda_B}\right)^{|l|} \exp\left(-\frac{r^2}{4\lambda_B^2}\right) {}_1F_1\left(\frac{1+l+|l|}{2} - \frac{E}{\hbar\omega}, 1+|l|; \frac{r^2}{2\lambda_B^2}\right) \qquad (24)$$

where ${}_1F_1(v, w; u)$ is the confluent hypergeometric function [11]. The spectrum can be computed numerically by finding the zeros v of this function for $u = R^2/2\lambda_B^2$ [12].

As a result of the singularity at the origin due to the centrifugal potential $l^2\hbar^2/2mr^2$ in (23), the WKB method cannot be applied directly to solve this equation. One can handle this problem by performing a Langer transformation [13] $x = -\ln(r^2/r_c^2)$. In fact, when this change of variable is made in (23), one obtains a new equation with no pole in the potential and no first derivative. An easy way to handle the singularity of the potential at the origin is to use a method developed by Fröman and Fröman [8, ch 1]. This method, called by its authors the phase-integral method with unspecified basis, can be regarded to be a generalization of the Langer transformation. Both methods can be used, for example, to justify the celebrated Langer substitution [14] in the case of the radial equation of the hydrogen atom. As we shall see, in our case (two dimensions) Langer substitution is unnecessary. We first transform equation (23) in order to eliminate the first derivative and to have dimensionless quantities. Let $\mu = \hbar\omega/2E$, $\rho_0 = R/r_c$ and $l_z = l\hbar/m\omega r_c^2 = l\mu$. Making the change of variable $\rho = r/r_c$ and setting $\varphi(r) = \varphi(\rho) = \rho^{-1/2}y(\rho)$ in (23), we obtain:

$$\frac{d^2y}{d\rho^2} = \left(-\frac{1}{\mu^2}Q^2(\rho) - \frac{1}{4\rho^2}\right)y(\rho) \qquad (25)$$

where $Q^2(\rho) = -\rho^2/4 + 1 - l_z - l_z^2/\rho^2$. The boundary conditions are:

$$y(\rho_0) = 0 \qquad \lim_{\rho \to 0} \rho^{-\frac{1}{2}}y(\rho) < \infty. \qquad (26)$$

For small μ, the last term in the parenthesis on the r.h.s. of (25) can be neglected as compared with the first (the interested reader is referred to [8] for the justification of this point). Let us set $a = 2(1 - l_z)$ and $c = \sqrt{1 - (2l_z/a)^2}$. Far from the zeros $\rho_{\min} = \sqrt{a(1-c)}$ and

$\rho_{\max} = \sqrt{a(1+c)}$ of $Q^2(\rho)$, the approximate solution of (25) is [8]:

$$y(\rho) = |Q^2(\rho)|^{-1/4} \left(C_+ \exp \left(\frac{1}{\mu} \int^\rho d\rho' \sqrt{-Q^2(\rho')} \right) \right.$$
$$\left. + C_- \exp \left(-\frac{1}{\mu} \int^\rho d\rho' \sqrt{-Q^2(\rho')} \right) \right) \tag{27}$$

where C_+ and C_- are arbitrary constants. If $l_z > \frac{1}{2}$, $Q^2(\rho) < 0$ for all ρ's and thus approximation (27) is valid everywhere. The integral in the exponentials diverges at zero and (26) implies that $C_+ = 0$ and $C_- = 0$. There are therefore no semiclassical solutions of (25) and (26) for such l_z's, and we can restrict our discussion to the classically allowed region $l_z \leqslant \frac{1}{2}$.

As noted above, when $\rho_0 > 1$ the two turning points, $\rho_{\min}$ and $\rho_{\max}$, tend to coalesce as $l_z \to \frac{1}{2}$; but it is well known that the standard WKB or phase-integral analysis fails to give approximations valid no matter how close they are to the turning points. We are thus led to use the so-called comparison equation method [7, 8] which gives uniform approximation for this case. The main motivation to use this method is that it connects our problem nicely with the previously solved problem of the semi-infinite plane. The approximate solution of (25) is written in terms of a function $f(\sigma)$ solution of a simpler equation. We shall choose this simpler 'comparison equation' to be:

$$\frac{d^2 f}{d\sigma^2} = \left(\sigma^2 - \frac{1}{\epsilon} \right) f(\sigma) \tag{28}$$

where ϵ is a parameter to be determined later. The solution $y(\rho)$ of (25) is obtained by multiplying $f(\sigma)$ by a slowly varying amplitude and allowing its argument σ to depend weakly on ρ. In other words, we look for solutions of the form $y(\rho) = A(\rho) f(\sigma(\rho))$. The equation obeyed by the mapping function $\sigma(\rho)$ becomes simpler if we choose $A(\rho) = (\frac{d\sigma}{d\rho})^{-1/2}$, and reads:

$$\frac{1}{\mu^2} Q^2(\rho) + \frac{1}{4\rho^2} = \left(\frac{d\sigma}{d\rho} \right)^2 \left(\frac{1}{\epsilon} - \sigma^2(\rho) \right) - \left(\frac{d\sigma}{d\rho} \right)^{1/2} \frac{d^2}{d\rho^2} \left(\frac{d\sigma}{d\rho} \right)^{-1/2}. \tag{29}$$

If $(\frac{d\sigma}{d\rho})^{-1/2}$ varies suffisciently slowly and if μ is small enough, the second term on the r.h.s. and the second term on the l.h.s. of equation (29) can be neglected:

$$\frac{1}{\mu^2} Q^2(\rho) \simeq \left(\frac{d\sigma}{d\rho} \right)^2 \left(\frac{1}{\epsilon} - \sigma^2(\rho) \right) \tag{30}$$

(for more details and justifications of this approximation see [8]).

Let us define by analogy with (5) the classical radial action variable $I_r(\rho)$ for $\rho_{\min} \leqslant \rho \leqslant \rho_{\max}$:

$$I_r(\rho) = \frac{1}{\pi} \int_{r_c \rho_{\min}}^{r_c \rho} dr \sqrt{2mE - \frac{1}{r^2} \left(l\hbar + \frac{m\omega}{2} r^2 \right)^2} = \frac{\hbar}{\pi \mu} \int_{\rho_{\min}}^\rho d\rho' \, Q(\rho'). \tag{31}$$

For $\pm\rho \geqslant \pm\sqrt{a(1 \pm c)}$, $Q^2(\rho)$ is negative and the action is purely imaginary:

$$I_r(\rho) = \frac{-i\hbar}{\pi \mu} \int_{\sqrt{a(1\pm c)}}^\rho d\rho' \sqrt{-Q^2(\rho')}. \tag{32}$$

An easy calculation gives:

$$\frac{\pi}{\hbar} I_r(\rho) = \frac{a}{4\mu} \left(\sqrt{c^2 - \left(\frac{\rho^2}{a} - 1 \right)^2} + \arccos \left(\frac{1}{c} - \frac{\rho^2}{ac} \right) \right.$$
$$\left. - \sqrt{1 - c^2} \arccos \left(\frac{(1-c^2)a}{c\rho^2} - \frac{1}{c} \right) \right). \tag{33}$$

This formula is correct for all ρ's if one defines $\sqrt{1 - u^2} = -i\sqrt{u^2 - 1}$ if $|u| > 1$ and $\arccos(u) = \mp i \operatorname{arccosh}(|u|)$ if $\pm u > 1$.

For the above analysis to be meaningful, the mapping $\rho \mapsto \sigma$ has to be one to one, i.e. $\frac{d\sigma}{d\rho}$ and $\frac{d\rho}{d\sigma}$ must never vanish. From (30) and assuming $\frac{d\sigma}{d\rho} < 0$, it follows that $\sigma(\rho_{\min}) = 1/\sqrt{\epsilon}$ and $\sigma(\rho_{\max}) = -1/\sqrt{\epsilon}$. By integrating (30) and making the change of variable $\xi = \sqrt{\epsilon}\sigma - 1$, we obtain if $\rho \leqslant \rho_{\max}$:

$$I_r(\rho) = \frac{\hbar}{\pi\epsilon} \int_{\xi(\rho)}^{0} d\xi \sqrt{-\xi(\xi + 2)} = I_x(\xi(\rho) + 1) \tag{34}$$

where $\xi(\rho) = \sqrt{\epsilon}\sigma(\rho) - 1$ and $I_x(\xi + 1)$ is the action of the semi-infinite plane (see (5)), which is given by (17) for all ξ's (with the same conventions as above for the square root and the arccos functions). If $\rho > \rho_{\max}$, so that $\xi(\rho) < -2$, (34) is still correct if the upper bound of integration 0 is replaced by -2. Using (31), (32), (34) and (17) one can show that the mapping function takes the following forms when ρ tends to 0, ∞, $\rho_{\min}$ and $\rho_{\max}$ respectively:

$$\sqrt{\epsilon}\sigma(\rho) \simeq \left| 2\epsilon l \ln\left(\frac{\rho}{\rho_{\min}}\right) \right|^{1/2} \qquad \text{if } \rho \ll \rho_{\min} \tag{35}$$

$$\sqrt{\epsilon}\sigma(\rho) \simeq -\sqrt{\frac{\epsilon}{2\mu}}\rho \qquad \text{if } \rho \gg \sqrt{a} \tag{36}$$

$$\sqrt{\epsilon}\sigma(\rho) \mp 1 \simeq \left(\frac{a\sqrt{c\epsilon}}{4(1 \mp c)\mu}\right)^{2/3}\left(-\frac{\rho^2}{a} + 1 \mp c\right) \text{if } \left|\frac{\rho^2}{a} - 1 \pm c\right| \ll c(1 \mp c). \tag{37}$$

The parameter ϵ is obtained by setting $\rho = \rho_{\max}$ and $\xi(\rho_{\max}) = -2$ in (34). Let $\theta(l) = 0$ for $l < 0$ and 1 for $l \geqslant 0$, then

$$\frac{1}{2\epsilon} = \frac{1}{2\mu} - l\theta(l). \tag{38}$$

The comparison equation (28) is transformed into equation (8) by means of a change of variable $\xi = \sqrt{\epsilon}\sigma - 1$. Moreover, using (30) and (35), one can show that $(d\sigma/d\rho)^{-1/2} \sim \rho^{1/2}|2\ln(\rho/\rho_{\min})/l|^{1/4}$ when $\rho \to 0$. The second condition in (26) implies that $\rho^{-1/2}(d\sigma/d\rho)^{-1/2}f(\sigma(\rho))$ has a finite limit when $\rho \to 0$, and therefore that $f(\sigma) \to 0$ when $\sigma \to \infty$. We can thus use the results of section 2 to determinate the approximate solution of (25) and (26). It is given (up to an arbitrary multiplicative constant) by:

$$y_{\text{WKB}}(\rho) = \left(\frac{-\xi(\rho)^2 - 2\xi(\rho)}{Q^2(\rho)}\right)^{1/4} f_{\text{WKB}}(\xi(\rho)) \tag{39}$$

where $\xi(\rho) = \sqrt{\epsilon}\sigma(\rho) - 1$ and $f_{\text{WKB}}(\xi)$ is the WKB solution of (8) vanishing at infinity and satisfying the boundary condition (10) with $\xi_0 = \xi(\rho_0) + 1 = \sqrt{\epsilon}\sigma(\rho_0)$. Using (13), (14), (16), (18), (20) and (37), the semiclassical wavefunction of the disk is obtained (η is a small parameter):

$$\varphi(\rho) = (-\rho^2 Q^2(\rho))^{-1/4} \exp\left(\frac{i}{\hbar}\pi I_r(\rho)\right) \qquad \text{if } \rho \leqslant \rho_{\min} - \eta$$

$$= \frac{2\sqrt{\pi}}{(a^2(c - c^2)\mu)^{1/6}} \text{Ai}\left(\left(\frac{a\sqrt{2c}}{4(1 - c)\mu}\right)^{2/3}\left(-\frac{\rho^2}{a} + 1 - c\right)\right)$$

$$\text{if } \rho_{\min} - \eta \leqslant \rho \leqslant \rho_{\min} + \eta$$

$$= 2(\rho^2 Q^2(\rho))^{-1/4} \sin\left(\frac{\pi}{\hbar}I_r(\rho) + \frac{\pi}{4}\right) \qquad \text{if } \rho_{\min} + \eta \leqslant \rho \leqslant \rho_{\max} - \eta$$

$$= \frac{2\sqrt{\pi}}{(a^2(c+c^2)\mu)^{1/6}} \left\{ \sin\left(\frac{\pi}{2\epsilon}\right) \text{Ai}\left(\left(\frac{a\sqrt{2c}}{4(1+c)\mu}\right)^{2/3} \left(\frac{\rho^2}{a} - 1 - c\right) \right) \right.$$

$$\left. + \cos\left(\frac{\pi}{2\epsilon}\right) \text{Bi}\left(\left(\frac{a\sqrt{2c}}{4(1+c)\mu}\right)^{2/3} \left(\frac{\rho^2}{a} - 1 - c\right) \right) \right\}$$

if $\rho_{\max} - \eta \leqslant \rho \leqslant \rho_{\max} + \eta = (-\rho^2 Q^2(\rho))^{-1/4}$

$$\left\{ \sin\left(\frac{\pi}{2\epsilon}\right) \exp\left(-\frac{i}{\hbar}\pi I_r(\rho)\right) + 2\cos\left(\frac{\pi}{2\epsilon}\right) \exp\left(\frac{i}{\hbar}\pi I_r(\rho)\right) \right\}$$

if $\rho \geqslant \rho_{\max} + \eta.$ \hfill (40)

This semiclassical approximation of equation (23) becomes better as the magnetic field tends to zero. In fact, in this limit the energies E must tend to their finite zero-field values and therefore $\mu = \hbar\omega/2E$ approaches zero. The semiclassical analysis is thus expected to work particularly well for low fields.

3.3. The semiclassical spectrum

Let $N_\Phi = m\omega R^2/2\hbar$ be the magnetic flux through the disk in units of the quantum flux Φ_0. The energy $1/2\epsilon$ in (38) must coincide with the semi-infinite plane energy (11). Fixing N_Φ, n_x and l, the energy levels $E/\hbar\omega = 1/2\mu$ of the disk are thus given by solving the two coupled equations:

$$\frac{1}{2\mu} = h_{n_x}(\xi_0) + l\theta(l)$$

$$I_x(\xi_0) = I_r((2N_\Phi\mu)^{1/2}).$$ \hfill (41)

The second equation is obtained by setting $\rho = \rho_0 = (2N_\Phi\mu)^{1/2}$ and $\xi_0 = \xi(\rho_0) + 1$ in (34). As for the semi-infinite plane there are no levels $h_{n_x}(\xi_0)$ with $\xi_0 > 1$, we must have $\rho_0 \geqslant \rho_{\min}$. Equivalently, the angular momentum l_z satisfies the classical conditions $-\rho_0^2/2 - \rho_0 \leqslant l_z \leqslant \frac{1}{2}$ if $\rho_0 > 1$ and $-\rho_0^2/2 - \rho_0 \leqslant l_z \leqslant -\rho_0^2/2 + \rho_0$ if $\rho_0 \leqslant 1$. Using (41), we see that if $l \leqslant 0$ the energies $E/\hbar\omega = 1/2\mu \gg n_x + \frac{1}{2}$ are associated with values of ξ_0 very close to 1, i.e. with values of ρ_0 and l_z nearly equal to $\rho_{\min}$ and $-\rho_0^2/2 \mp \rho_0$ respectively. These energies correspond to the whispering gallery orbits, i.e. to the second branch of $h_{n_x}(\xi_0)$. An approximation for these high energies can be obtained by taking $l_z = -\rho_0^2/2 \mp \rho_0$. Since $l_z = l\mu$ and $\rho_0^2 = 2N_\Phi\mu$ this implies:

$$\frac{E}{\hbar\omega} \simeq \frac{1}{4N_\Phi}(|l| - N_\Phi)^2.$$ \hfill (42)

This expression is valid for large negative values of l. In other words, for such l's the energy E (for fixed R) varies like $(|l| - N_\Phi)^2$ with the magnetic field; this quadratic variation is indeed observed on the numerical spectrum showed in figure 5. Note that $l_z \to 0$ when $l \to -\infty$.

Figure 4 shows for $N_\Phi = 20$ and $n_x = 0$ the semiclassical energies calculated numerically by solving the coupled equations (41) and by using (17), (33) and results of section 2. The comparison with the exact numerical spectrum (full curve) show a surprisingly good agreement for these low energies and high N_Φ. From the above arguments (sections 2.2 and 3.1), it is clear that if $\rho_0 > 1$, the EBK quantization rules give an incorrect gap in the spectrum. The discontinuous transition from bulk to edge levels in the EBK spectrum (dotted curve) occurs when $\rho_0 = \rho_{\max}$, i.e. when $l_z = -\rho_0^2/2 + \rho_0$; the
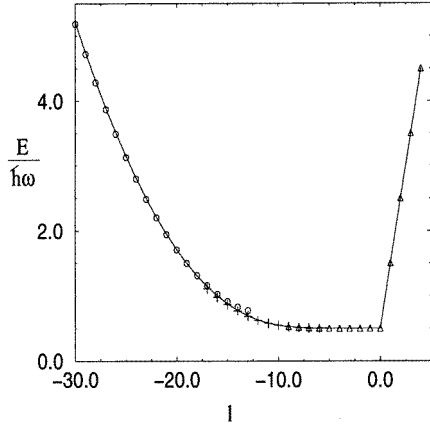
Figure 4. The energy spectrum of the disk as function of the angular momentum ($N_\Phi = 20$): circles represent the zeros of the third branch, pluses represent the zeros of the fourth branch and triangles represent the zeros of the fifth branch. The full and dotted curves represent respectively the exact and the EBK spectrum.
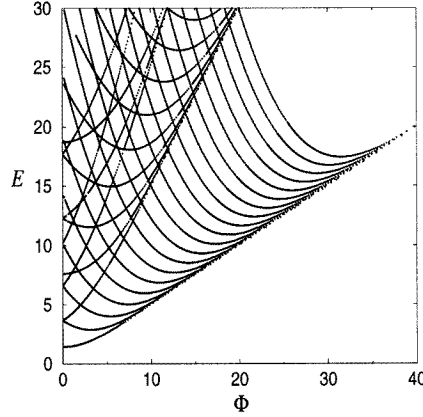
Figure 5. The energy spectrum of the disk as function of the magnetic flux. The energy E in the vertical axis is in units of $2\hbar^2/mR^2$.

EBK energies $(1/2\mu)_{EBK}$ tend to $I_r(\rho_{max}) + l\theta(l) = n_x + l\theta(l) + \frac{3}{4}$ when $\rho_0 \to \rho_{max}-$, whereas they are equal to the Landau levels $n_x + l\theta(l) + \frac{1}{2}$ if $\rho_0 > \rho_{max}$. The value of the angular momentum separating the edge and bulk levels is thus given for the n_xth band by $l = -N_\Phi + \sqrt{4N_\Phi(n_x + l\theta(l) + \frac{3}{4})}$. One can conclude that the EBK rules (or any trace formula based on them) badly reproduce the spectrum for big N_Φ's. Blaschke and Brack [15] did independently reach similar conclusions using periodic orbits techniques in a recent work. These authors calculated the density of states of the disk in magnetic field by replacing the Maslov index by a smooth function they determine numerically.

Let us discuss in more details the IQHE and low-field regimes.

3.3.1. The IQHE regime $N_\Phi \gg 1$. For negative values of the angular momentum l such that $|l| \gg N_\Phi$, the levels can be approximated as in equation (42). Increasing l, $\rho_0^2/a = (1/N_\Phi\mu + |l|/N_\Phi)^{-1}$ moves away from its minimum value $\rho_{min}^2/a = 1 - c$, so that we go towards lower energies. When ρ_0^2/a is between but not too close to $1 - c$ and $1 + c$ and if $n_x \ll N_\Phi$, the energy $1/2\mu = 1/2\epsilon$ is much smaller than N_Φ. This corresponds to values of $|l|$ of the order of N_Φ. For such $|l|$'s one has $\rho_0^2/a \simeq N_\Phi/|l|$ and the action $I_r(\rho_0)$ can be quantized according to the EBK rules (see the item (iii) of section 2.3). Increasing further l, the states transform gradually into Landau-like states located far apart from the boundary. For angular momenta l such that $|l| \ll N_\Phi$, ρ_0^2/a is large and thus ξ_0 is a large negative number (see (36)). It follows from the analysis of section 2 that $h_{n_x}(\xi_0)$ is close to the Landau level $n_x + \frac{1}{2}$. In other words, levels with small angular momenta $|l| \ll N_\Phi$ practically do not feel the boundary. For negative l's, the level is close to the n_xth Landau level, for positive l's it is close to the $(n_x + l)$th Landau level. Since $n_x \geqslant 0$, there are no bulk levels with positive angular momenta $l > n$ near the nth Landau level. This fact can be seen on the exact spectrum shown in figure 5 by following the levels from $B = 0$. Each time n is decreased by one, one level of positive l is removed. One finds for l_z the upper bound $l_z \leqslant \frac{n}{2n+1}$, which again gives the classical condition $l_z \leqslant \frac{1}{2}$ when $n \to \infty$.

3.3.2. The low-field regime $N_\Phi \ll 1$. When $\omega \to 0$, the exact energies of the states of angular momentum l approach their zero-field values $E_0 = \hbar^2 j_l^2 / 2mR^2$, where j_l are the zeros of the Bessel function of order l (note that due to the time-reversal symmetry, states with opposite l are degenerate in energy at $B = 0$, i.e. $j_l = j_{-l}$). For small fields and fixed l, $\mu = \hbar\omega/2E = O(\omega)$, $l_z = l\mu$ and $\rho_0 = (2N_\Phi\mu)^{1/2}$ are small. By expanding the action $I_r(\rho)$ in (33) for $\rho = \rho_0$ up to second order in the field we find

$$\frac{2\pi}{\hbar|l|} I_r(\rho_0) = 2\sqrt{z_0 - 1} - 2\arccos(z_0^{-1/2}) + \frac{1 - z_0^{-1}}{\sqrt{z_0 - 1}}\left(\delta z - \frac{2N_\Phi}{l}\right)$$

$$+ (z_0 - 1)^{-3/2}\left(\left(-1 + \frac{3}{z_0} - \frac{2}{z_0^2}\right)\left(\frac{\delta z^2}{4} - \frac{N_\Phi \delta z}{l}\right)\right.$$

$$\left. + \frac{N_\Phi^2}{3l^2}\left(-z_0 - 3 + \frac{12}{z_0} - \frac{8}{z_0^2}\right)\right) + O(\omega^i \delta z^j) \tag{43}$$

where $z = 2N_\Phi/\mu l^2 = 2mR^2 E/\hbar^2 l^2$, $\lim_{\omega\to 0} z = z_0$, $\delta z = z - z_0$ and $i + j \geqslant 3$. Since $\mu I_r(\rho_0) = \mu I_x(\xi_0) \to 0$ when $\omega \to 0$, one can deduce from (38) and (17) that $\xi_0 \to 1$ when $\omega \to 0$. Therefore we can use in this limit the 'generalized EBK rules' developed in part (ii) of section 2.3 to quantize the action $I_r(\rho_0)$. Taking $\omega = 0$ in (43), we obtain that the square root energy $\sqrt{2mR^2 E_0/\hbar^2} = \sqrt{l^2 z_0}$ is equal to the first term of the uniform asymptotic expansion of the zeros of the Bessel function of order l, i.e. it satisfies (see [11]):

$$\frac{\pi I_r(\rho_0)}{\hbar} = |l|\sqrt{z_0 - 1} - |l|\arccos(z_0^{-1/2}) = \tfrac{2}{3}(-a_{n_x})^{3/2}. \tag{44}$$

Our semiclassical analysis gives thus the exact zero-field energies up to higher terms in this asymptotic expansion, i.e. with an error of the order of 1% for the lowest energies (including those with $l = 0$) [11]. As noted in [16], by using the EBK rules to quantize the action (i.e. replacing the r.h.s. of (44) by $\pi(n_x + \frac{3}{4})$) good approximations of the exact zero-field energies are already obtained. We can conclude (in accordance with [15]) that the corrections to the EBK spectrum provided by a proper treatment of the whispering gallery orbits are small. For small but non-zero ω, the action $I_r(\rho_0)$ remains quantized through the same rules and is equal (in this approximation) to its zero-field value (44). It immediately follows from (43) that $\delta z = 2N_\Phi/l + O(\omega^2)$. Substituting this value into the action we obtain the energies up to second order in ω:

$$\frac{2mR^2 E}{\hbar^2} = j_l^2 + 2lN_\Phi + \frac{N_\Phi^2}{3}\left(1 + \frac{2l^2}{j_l^2}\right) + O(\omega^3). \tag{45}$$

This result agrees with recent semiclassical perturbative calculations at low fields [17]. However, it does not coincide with the exact second-order perturbation theory result of Dingle [18], where a different factor multiplying N_Φ^2 in (45) was obtained (the two expressions being asymptotically equal for large energies). This discrepancy should affect the magnetic susceptibility, which is a measure of the field dependence of the levels, for low Fermi energies. If the energy is sufficiently large, one can however use (45) to study the level crossings at low N_Φ's. The values N_Φ at which there are level crossings are given by the solutions of the second degree equation:

$$\frac{2N_\Phi^2}{3}\left(\frac{l_1^2}{j_{l_1}^2} - \frac{l_2^2}{j_{l_2}^2}\right) + 2N_\Phi(l_1 - l_2) + j_{l_1}^2 - j_{l_2}^2 = 0 \tag{46}$$

where j_{l_1} and j_{l_2} are zeros of the Bessel functions of order respectively l_1 and l_2.

3.4. Charge transport

Suppose that one introduces an Aharonov–Bohm flux line through the origin O, and studies the transport of charges induced by varying the flux ϕ. The vector potential is changed by $\boldsymbol{A} \to \boldsymbol{A}_0 + \frac{\phi}{2\pi r}\boldsymbol{e}_\theta$, where $\boldsymbol{A}_0$ is the vector potential created by the uniform magnetic field. The Schrödinger equation for this system is still of the form (23) but with l replaced by $l + \alpha$, where $\alpha = \phi/\Phi_0$. Therefore all our results still apply modulo this substitution. The spectrum is identical for α's which differ by integer values (gauge invariance). Changing continuously the flux ϕ is equivalent to an electromotive force (e.m.f.) through the system. Consider α varying continuously from 0 to 1. Then all eigenstates and energies of the system evolve adiabatically. Edge levels lower their energies and fall (at $\alpha = 1$) into the level situated just below them. Bulk levels are almost not affected except those with positive l, whose energies $E \simeq \hbar\omega(n_x + l + \alpha + \frac{1}{2})$ are increased by $\hbar\omega$, the electron jumping from one Landau-like level into another. Introducing the Fermi energy E_F for an independent electron gas at zero temperature, we see that the effect of changing the flux by one unit is to remove n electrons from the centre of the disk and to transfer them to the boundary if E_F is between the nth and the $(n+1)$th Landau level (as in Laughlin's argument [4]). This conclusion is not specific to the disk geometry, since it is due to positive l states which are almost insensitive to the boundary when $N_\Phi \gg 1$.

4. Conclusion

We have presented a semiclassical calculation of the energy spectrum and the eigenfunctions of an electron in a perpendicular and uniform magnetic field for the half-plane and the disk geometries. These situations are the simplest to describe features due to the presence of both a perpendicular field and a boundary. In fact, explicit calculations can be made in both cases using the existence of a constant of motion resulting from the symmetry of the system (namely the momentum in the direction parallel to the boundary for the half-plane, and the angular momentum for the disk). One can then reduce these two-dimensional problems into one-dimensional ones and use asymptotic methods to solve them.

Because of the inherent splitting between bulk and edge classical trajectories, the EBK quantization rules fail to give the correct gradual transition between Landau-like bulk levels and edge levels. As noted in [15], a more correct semiclassical approach must take into account the coalescence of the caustics with the boundary due to edge orbits making nearly full circles before being reflected or to bulk orbits nearly touching the boundary. This removes the EBK gap between the bulk and edge energies and results in a semiclassical spectrum which approximates surprisingly well the lowest levels, as far as we checked from our numerical calculations. Under usual boundary conditions (such as the Dirichlet case considered here), the notion of edge and bulk states is no longer well-defined as in classical mechanics; to restore a precise meaning of such a dichotomy in quantum mechanics and describe for instance the transition from edge to bulk states in the context of the IQHE, one has to consider more general boundary conditions [19] pertaining to the family defined by Atiyah *et al* [20].

The extension of our results to general (non-integrable) billiards with smooth boundaries could be made by using the more elaborate path-integration semiclassical methods, or, for almost circular billiards, by expanding the wavefunction on the WKB disk wavefunction. The existence in zero-field of regimes of localization of the wavefunction in the angular momentum space was shown recently for almost circular billiards with a rough boundary [21]. The most general approach would be to try to derive a specific trace formula for

billiards in magnetic field wich takes the coalescence of the caustics with the boundary into account. Recent works [22] on the diffraction contribution to the semiclassical spectral density for general billiards in zero-field can be of relevance to this problem.

Acknowledgments

References

[1] Levy L P, Reich D H, Pfeiffer L and West K 1993 *Physica* **189B** 204
[2] Nakamura K and Thomas H 1988 *Phys. Rev. Lett.* **61** 247
[3] Ullmo D, Richter K and Jalabert R A 1995 *Phys. Rev. Lett.* **74** 383
   for a review see Richter K, Ullmo D and Jalabert R A 1996 *Phys. Rep.* **276** 1
[4] Laughlin R B 1981 *Phys. Rev.* B **23** 5632
   MacDonald A H and Středa P 1984 *Phys. Rev.* B **29** 1616
   Halperin B I 1982 *Phys. Rev.* B **25** 2185
[5] Brillouin M L 1926 *J. Physique* **7** 355
   Keller J B 1958 *Ann. Phys., NY* **4** 180
[6] Isihara A and Ebina K 1988 *J. Phys. C: Solid State Phys.* **21** L1079
[7] Berry M V and Mount K E 1972 *Rep. Prog. Phys.* **35** 315
[8] Fröman N and Fröman P O 1995 *Phase-integral Method: Allowing Nearlying Transition Points (Springer Tracts in Natural Philosophy 40)*
[9] Miller S C and Good R H 1953 *Phys. Rev.* **91** 174
[10] Bender C M and Orszag S A 1978 *Advanced Mathematical Methods for Scientists and Engineers* (New York: McGraw-Hill)
[11] Abramowitz M and Stegun I A (ed) 1972 *Handbook of Mathematical Functions* (Washington, DC: National Bureau of Standards)
[12] Geerinckx F, Peeters F M and Devreese J T 1990 *J. Appl. Phys.* **68** 3435
[13] Langer R E 1937 *Phys. Rev.* **51** 669
[14] Kramers H A 1926 *Z. Phys.* **39** 828
[15] Blaschke J and Brack M 1997 *Phys. Rev.* A **56** 182
[16] Keller J B and Rubinow S I 1960 *Ann. Phys., NY* **9** 24
[17] Gurevich E and Shapiro B 1997 *J. Physique* I **7** 807
[18] Dingle R B 1952 *Proc. R. Soc.* A **212** 47
[19] Akkermans E, Avron J E, Narevich R and Seiler R 1998 *Eur. Phys. J.* B **1** 117
[20] Atiyah M F, Patodi V K and Singer I M 1975 *Math. Proc. Camb. Phil. Soc.* **77** 43
[21] Frahm K M and Shepelyansky D L 1997 *Phys. Rev. Lett.* **78** 1440
   Frahm K M 1997 *Phys. Rev.* B **55** 8626
[22] Primack H, Schanz H, Smilansky U and Ussishkin I 1996 *Phys. Rev. Lett.* **76** 1615
   Sieber M, Pavloff N and Schmit C 1997 *Phys. Rev.* E **55** 2279